Supporting Information

Biofunctionalization of Large Gold Nanorods Realizes Ultrahigh-Sensitivity Optical Imaging Agents

*Elliott D. SoRelle,[1,2,3] Orly Liba,[1,3,4] Zeshan Hussain,[1,3] Milan Gambhir,[1,3] and Adam de la Zerda[1,2,3,4] **

[1]Molecular Imaging Program at Stanford, Bio-X Program, and [2]Biophysics Program, [3]Departments of Structural Biology, and [4]Electrical Engineering, Stanford University, Palo Alto, California 94305

***Correspondence should be directed to adlz@stanford.edu**

DETAILED EXPERIMENTAL METHODS

Particle Synthesis. Gold nanorods within two different size regimes were synthesized using modified versions of two previously reported seed-mediated growth methods. GNRs (~50 x 15 nm) were prepared according to an original method by Nikoobakht and El-Sayed.[23] Briefly, a seed solution was prepared by adding 5 mL 0.2 M of CTAB (≥ 98%, TCI, CAS# 57-09-0) and 5 mL of 0.0005 M $HAuCl_4$ (≥ 49.0% Au basis, Sigma-Aldrich, CAS# 16961-25-4) with gentle stirring, after which 0.6 mL of 0.01 M $NaBH_4$ (≥ 99%, Fluka, CAS# 16940-66-2) was added. This solution was stirred for 2 min at 25°C prior to use. Two growth solutions (GNRs I and II) were prepared by adding 5 mL of 0.2 M CTAB to 225μL (I) or 275μL (II) of 0.004 M $AgNO_3$ (99.9999% trace metal basis, Aldrich, CAS# 7761-88-8) at 25°C under gentle stirring. 5 mL of 0.001 M $HAuCl_4$ was then added to each growth solution and mixed. Then, 70 μL of 0.0788 M L-Ascorbic Acid (reagent grade, Sigma, CAS# 50-81-7) was mixed into each solution. Finally, 12 μL of the seed solution was stirred into each growth solution and the solutions were left undisturbed at 30°C for 2 h. LGNRs (~90 x 30 nm) were prepared by adapting a two-surfactant method reported by the Murray group at the University of Pennsylvania.[24] Briefly, 9.0g CTAB and 1.234g sodium oleate (NaOL, ≥ 97%, TCI, CAS# 143-19-1) were added to 250 mL of H_2O at 50°C and stirred until dissolved. The temperature was then decreased to 30°C. Once this solution reached 30°C, either 25 mL (LGNRs I) or 50 mL (LGNRs II) of 0.004 M $AgNO_3$ was added. Each solution was left undisturbed for 15 min, after which 250 mL of 0.00086 M $HAuCl_4$ was added to each and stirred for 90 min at 700 rpm. During this time, the yellow-gold solution growth solutions turned colorless. A seed solution was also prepared during this time by adding 5 mL 0.2 M CTAB, 5 mL 0.000043 M $HAuCl_4$, and 0.6 mL of 0.01 M $NaBH_4$ + 0.4 mL H_2O. This seed solution was aged for 30 min prior to use. 90 min after the addition of $HAuCl_4$ to the growth solutions, 2.1 mL of 12.1 N hydrochloric acid (HCl, Fisher, CAS# 7647-01-0) was added to each growth solution and stirred at 400 rpm for 15 min. 1.25 mL of 0.064 M ascorbic acid was added to each growth and stirred vigorously (1200 rpm) for 30 seconds. Finally, 0.1 mL of aged seed solution was added to each growth (also at 1200 rpm stirring), and each growth solution was left undisturbed without stirring for 12 h at 30°C. Four different batches of GNRs (GNRs I, GNRs II, LGNRs I, and LGNRs II) were made using the protocols described above. While the protocols produce particles within distinct size regimes, GNRs I and LGNRs I both exhibited ~750 nm longitudinal surface plasmon resonance (LSPR) while GNRs II and LGNRs II exhibited ~ 800 nm LSPR, facilitating spectral and stability comparisons between particles.

Particle Coating. Each of the four (L)GNR batches was prepared with three different surface coatings: CTAB, $mPEG_{5000}$ –SH (MW ~ 5000 Da, Laysan Bio, Arab, AL), or Poly(sodium 4-styrenesulfonate) (PSS, MW ~ 70 kDa, Aldrich, CAS# 25704-18-1). GNRs-CTAB were taken directly from as-synthesized growth solutions. (L)GNRs-mPEG were prepared using a modified version of a previous protocol[29] by incubating as-synthesized (L)GNRs-CTAB solutions with 1 mg/mL $mPEG_{5000}$-SH for 24 hrs at room temperature with gentle mixing. LGNRs-PSS (Large GNRs only) were prepared by adding 0.1 mL of 0.001 M PSS to 1 mL of GNRs-CTAB. Both GNRs-mPEG and GNRs-PSS were washed once by centrifugation (2550 x g for 10 min at 25°C in an Eppendorf 5417R microcentrifuge) to remove excess CTAB. Because this step was required to remove excess CTAB, measurements of $mPEG_{5000}$-SH or PSS particles start at 1x wash rather than the 0x wash step at which CTAB GNR measurements start. This step was taken to maintain the integrity of comparisons of particle stability with respect to surface coating and rounds of washing.

Particle Stability Characterization. The four batches of unwashed GNRs-CTAB were initially characterized in terms of spectral characteristics, physical size, and surface potential. Spectra were measured using a Cary 6000i spectrophotometer. Note that all (L)GNR batches were adjusted to the same optical density (OD) prior to characterization for comparison. Size distributions and average dimensions for each (L)GNR batch were determined from images taken by a JEOL TEM 1400 electron microscope. Zeta potential for each batch was measured using a Malvern Zetasizer Nano ZS. In addition to this initial characterization, spectra and zeta potential for each (L)GNR batch with each surface coating were measured after each of four wash steps to characterize particle stability in distilled deionized (DDI) H_2O. A single wash step consisted of the following: centrifugation of 1 mL (L)GNR solution (2550 x g for 10 min at 25°C), removal of 950 μL supernatant, and resuspension of the GNR pellet with 950 μL fresh DDI H_2O. Thus, one wash resulted in a ~20-fold decrease in concentration of any small molecules in the supernatant. For example, the concentration of CTAB in as-synthesized LGNRs is ~45 mM:

9.0 g CTAB (MW = 364.45 g/mol) into ~550 mL growth solution =
0.0247 mol CTAB / 0.550 L =
0.045 M CTAB

After one wash, the concentration of CTAB in solution is reduced to 2.25 mM. A second wash further reduces the CTAB concentration to 0.11 mM (at which point the LGNRs irreversibly aggregated). Additional batches of LGNRs (93 x 33 nm) and GNRs (40 x 10 nm, NanoPartz, Loveland, CO) prepared with each coating described above were also analyzed using dynamic light scattering (DLS) with a Malvern ZetaSizer Nano ZS and Vis-NIR spectrometry to verify successful surface coating after 1x washing.

PEG-SH Binding Studies. Both GNRs and LGNRs were separately incubated with Biotin-PEG_{5000}-SH to produce GNRs-PEG-Biotin and LGNRs-PEG-Biotin, respectively. These particles were washed 1x and prepared to OD 5 and OD 10, respectively. 50 μL of each particle solution was then incubated with 10 μL of OD 5 NeutrAvidin-coated 10 nm Gold Nanospheres (GNS-NA, Nanopartz, Loveland, CO). GNRs-mPEG and LGNRs-mPEG were also incubated in identical fashion with GNS-NA. TEM images of GNS-NA incubated with each of these four particles (LGNRs-mPEG, LGNRs-PEG-Biotin, GNRs-mPEG, and GNRs-PEG-Biotin) were acquired to infer where PEG-SH reagents bind to (L)GNRs. Solutions of each of these four GNR-GNS incubations were also prepared to OD 1 and analyzed with Vis-NIR spectrometry and DLS to verify observations from TEM.

LGNR Biostability. In addition to the experiments described above, we also tested the stability of select LGNRs in biological serum. LGNRs coated with either $mPEG_{5000}$-SH (LGNRs-mPEG) or PSS (LGNRs-PSS) were incubated for 3 hrs with Fetal Bovine Serum (FBS) at room temperature. LGNR solutions were then centrifuged and washed 3x to remove excess FBS. LGNRs were characterized by absorbance spectra after each wash to assess serum stability.

We injected high doses of LGNRs-PSS-mPEG (up to 80 mg/kg) into female nude (nu^-/nu^-) and C57BL/6 mice (6-8 weeks old, Charles River Labs, Wilmington, MA). All animal experiments were performed in compliance with IACUC guidelines and with the Guidelines for the Care and Use of Research Animals established by the Stanford University Animal Studies Committee.

LGNR Biofunctionalization and Targeting. To demonstrate their utility for targeted biological studies, we tested whether LGNRs-PSS could be conjugated to retain binding capacity for specific ligands. Batch II (~800 nm LSPR) LGNRs-PSS at OD 20 was incubated with 1 mg/mL Biotin-PEG_{5000}-SH (MW ~ 5000 Da, NanoCS) for 24 hrs at room temperature (LGNRs-PSS-PEG-Biotin). LGNRs-PSS-PEG-Biotin were washed 2x to remove excess reagents from the supernatant. LGNRs-PSS-mPEG were also prepared using the same approach. After preparation, 100 μL of each particle type was incubated with 100 μL of streptavidin-coated polystyrene beads (3 μm avg. diameter, 0.5% w/v, Spherotech, product # SVP-30-5) and 10 μL FBS for 1 hr with 1500 rpm vortexing using a Multitherm tabletop shaker (Benchmark, Edison, NJ). After the incubation, each GNR + bead solution was diluted to a total volume of 1 mL. Each solution was centrifuged for 20 sec at 1000 x g. This time and speed are insufficient to pellet free LGNRs, but the majority of beads and any associated particles do pellet under this condition. Because of the high affinity of the interaction between biotin and streptavidin, this method enabled us to determine whether LGNRs-PSS-PEG-Biotin were capable of specific binding to a streptavidin substrate in the presence of FBS. Photographs were taken of bead pellets and supernatant to qualitatively assess the presence of LGNR binding for each condition. Vis-NIR spectra were also taken of each supernatant to indirectly quantify LGNR binding to pelleted streptavidin-coated beads. A blocking assay to test the molecular nature of GNR binding was also performed by incubating the streptavidin beads with an excess (1 mg/mL) of free biotin (≥ 99%, Sigma-Aldrich, CAS: 58-85-5) prior to the addition of LGNRs.

LGNRs-PSS-PEG-Biotin were separately functionalized with targeting peptides for use in cell incubation experiments. LGNRs-PSS-PEG-Biotin (1 mL OD 10) were incubated with 100 μL of 1 mg/mL NeutrAvidin (Thermo Fisher, #31000) at 25°C for 30 min to produce LGNRs-PSS-PEG-Biotin-NA (hence simply called "LGNRs-NA"). LNGRs-NA were subsequently incubated with 2 μL of 1 mg/mL Biotin-PEG-RGD (Peptides International, Louisville, KY) to produce LGNRs-cRGD. These particles were washed by centrifugation as described above. LGNRs-cRAD were also prepared as a control for binding specificity in cell incubation experiments shown in Figure S13.

Cell Targeting Experiments. For cell targeting experiments, U87MG cells (~1 million cells per sample) were incubated for 30 min with various LGNRs (functionalized with cRGD, cRAD, or mPEG) at a final concentration of OD 5. Each sample was washed 3 times by centrifugation at 300 x g to pellet cells. After the final wash, cells from each incubation were transferred to microscope slides for dark-field imaging. Cells-only (subjected to the same washing protocol) were imaged as a control. A blocking assay was also performed by incubating cells with free cRGD prior to incubation with LGNRs-cRGD and washing.

OCT System Optics, Experiments, and Analysis. Solutions of GNRs and LGNRs (each from batch II) were prepared at 2 x 10^{10} nps/mL (equal to OD 1 for LGNRs and OD 0.125 for GNRs). Each (L)GNR solution was added to a glass capillary tube with a 400 μm inner diameter. Pairs of tubes containing equal concentrations of (L)GNRs were then imaged with a Ganymede High-Resolution SD-OCT system (ThorLabs, Newton, NJ). The OCT light source is a superluminescent diode (SLD) operating at 30 kHz and centered at 900 nm with a 200 nm full bandwidth. The system has 4 μm lateral and 2.3 μm axial resolution in water. OCT images of GNRs were acquired with an LSM03 lens (ThorLabs, Newton, NJ) and processed by averaging 100 frames in B-scan mode. After acquisition, fields of view (each 15,000 pixels) at the same focal depth within each sample tube were used to calculate mean OCT signal +/- standard deviation. Another field of view at the focal depth was acquired to quantify the system noise

level. The mean noise level was subtracted from the mean signal of each GNR solution to quantify relative OCT contrast for each particle. Subsets (600 pixels each) of each original FOV were used in two-tailed student's t-tests to compare the average signal from LGNRs versus GNRs of equivalent concentrations.

***Ex Vivo* Tissue Preparation and Imaging.** As described in the Experimental Section in the main text, LGNRs-PSS-mPEG were administered intravenously to female nude mouse. Imaging was performed with OCT prior to and following the injection. The mouse was euthanized 24 hours after the LGNR-PSS-mPEG injection, and tissues were collected for *ex vivo* analysis. These tissues were preserved in 10% formalin, sectioned into 5 μm thick histological sections, and stained via standard H&E protocols. These stained samples were imaged using a CytoViva hyperspectral dark-field microscope (CytoViva, Auburn, AL) to further validate both the presence and biostability of the injected LGNRs. LGNRs produce a scattering spectrum distinct from that of tissue and can thus be identified with the CytoViva, which employs a spectrophotometer with a detection range of 400-1000 nm and spectral resolution of 2.8 nm. Tissues were also resected and prepared from a control animal that was not injected with LGNRs for comparison.

SUPPORTING RESULTS

(L)GNR-PEG Surface Coating Studies. We further investigated the differences in LGNR and GNR stability through additional characterization with Vis-NIR spectrometry, Dynamic Light Scattering (DLS), and TEM. Absorbance measurements indicate that GNRs exhibit a red-shift (~20 nm) after incubation with mPEG-SH (Figure S5b) and LGNRs undergo a blue-shift (~10 nm) after incubation with PSS (Figure S5a). However, no clear resonance shifting is observed between LGNRs-CTAB and LGNRs-mPEG (Figure S5a). While LGNRs-CTAB and LGNRs-mPEG exhibit similar zeta potential and absorbance trends, DLS reveals that LGNRs-mPEG have a greater hydrodynamic radius (~10 nm greater) than LGNRs-CTAB (Table S2), which is consistent with successful PEG coating. In contrast, LGNRs-PSS exhibited ~35 nm greater hydrodynamic radius than LGNRs-CTAB (Table S2). Thus, PSS may provide a thicker, more complete coating than mPEG-SH for LGNRs, leading to improved stability. Interestingly, GNRs-mPEG exhibited ~40 nm greater hydrodynamic radius than GNRs-CTAB (Table S2) suggesting that, unlike for LGNRs, mPEG-SH can provide a sufficiently dense coating to improve GNR stability.

While DLS provided insight into stability differences between LGNRs-mPEG and LGNRs-PSS, we sought to gain a more mechanistic understanding of the stability difference between GNRs-mPEG and LGNRs-mPEG. Previous studies have suggested that CTAB binds preferentially to GNRs along the longitudinal {100} faces, leaving the end cap {111} faces of the GNRs relatively exposed.[S1,S2] Consequently, it is proposed that PEG-SH and other ligands preferentially bind to the exposed ends due to steric accessibility and reaction kinetics.[S3] Separately, it can be shown from calculations of carbon-carbon and carbon-oxygen bond lengths that the maximum outstretched length of $mPEG_{5000}$-SH is ~50 nm.[S4] Given these observations, we hypothesized that PEG_{5000}-SH reagents bound preferentially at the ends of LGNRs cannot sufficiently coat the GNR surface due to its greater size relative to the PEG chain length. However, the PEG chains are long enough to provide good coating for GNRs. To test this, we prepared GNRs-PEG-Biotin, GNRs-mPEG, LGNRs-PEG-Biotin, and LGNRs-mPEG and

incubated each type with NeutrAvidin-coated 10 nm gold nanospheres (GNS-NA, see Methods). This biotin-NeutrAvidin binding assay allowed us to infer the position of bound PEG-SH reagents on (L)GNR surfaces by observing which (L)GNR faces interact with GNS-NA. TEM images show that GNS-NA appear consistently closer to the end caps of LGNRs-PEG-Biotin than to the GNR longitudinal surfaces (Figure S6a, bottom row). By contrast, GNS-NA show no such preferential location when incubated with LGNRs-mPEG, and the particles in this sample even appear to show early indications of aggregation (Figure S6a, top row). There does not appear to be spatial correlation between GNS-NA and GNRs-mPEG, and the GNRs do not appear to have aggregated as in the LGNR-mPEG sample (Figure S6b, top row). By comparison, there does appear to be some colocalization of GNRs-PEG-Biotin with GNS-NA (Figure S6b, bottom row), although GNS-NA do not show obvious preference for GNR end caps as with LGNRs-PEG-Biotin. To confirm these TEM results, we took absorbance measurements of each incubation condition. Based on plasmonic hybridization effects, we hypothesized that preferential binding of GNS-NA to the ends of GNRs with PEG-Biotin would cause red-shifting due to the effective increase in particle aspect ratio.[S5,S6] LGNRs-PEG-Biotin incubated with GNS-NA exhibit a significant red-shift (~20 nm) relative to free LGNRs-mPEG (Figure S7b), consistent with the composite particle morphology observed in TEM. LGNRs-mPEG incubated with GNS-NA exhibit a similar red-shift, however they also show significant spectral broadening consistent with the early aggregation observed in TEM images (Figure S7b). GNRs-PEG-Biotin exhibit red-shifting relative to both free GNRs-mPEG and GNRs-mPEG incubated with GNS-NA (Figure S7c). This suggests that GNS-NA bind to GNRs-PEG-Biotin but not GNRs-mPEG. As a final validation of TEM and Vis-NIR results, we measured GNR-GNS composite particle diameters using DLS. LGNRs-PEG-Biotin incubated with GNS-NA show significantly greater average hydrodynamic diameter (127 ± 0.6 nm) than free LGNRs-mPEG (34.6 ± 0.5 nm), consistent with GNS conjugation (Table S3). The same effect is observed for GNRs-PEG-Biotin (d = 93.9 ± 9 nm) relative to GNRs-mPEG (d = 61.6 ± 7 nm) (Table S3). LGNRs-mPEG incubated with GNS-NA show an even greater hydrodynamic diameter (408 ± 5.4 nm) (Table S3), consistent with the small aggregates observed in TEM and the broadening seen in Vis-NIR. Interestingly, GNRs-mPEG incubated with GNS-NA exhibit smaller diameters (28.7 ± 0.1 nm) in bulk than free GNRs-mPEG, however this could be due to the presence of unbound 10nm GNS-NA reducing the average measured diameter.

Cell Targeting Experiments. Incubation of U87MG ($\alpha_V\beta_3^+$) cells with various functionalized LGNRs demonstrates molecularly-specific targeting capabilities. Cells incubated with LGNRs functionalized with cRGD (which binds with high affinity to $\alpha_V\beta_3$) exhibited greater average cellular uptake than non-specific LGNRs (LGNRs-PSS-mPEG and LGNRs-cRAD). Moreover, cells that were blocked with free cRGD prior to incubation with LGNRs-cRGD also exhibited lower levels of particle uptake (Figure S13). Collectively, these results indicated that the increased uptake of LGNRs-cRGD was due to molecular specificity.

Validation of LGNR *iv vivo* Stability. The LGNRs used in this experiment exhibited a longitudinal plasmon resonance at 804 nm. This plasmonic peak overlapped significantly with our OCT system's light source and spectral detection range (800-1000 nm), which led to a strong contrast enhancement from LGNRs in circulation following injection. This contrast increase was observed in numerous blood vessels within the imaged region of the mouse ear (Figure 5d). It is important to note that this increase in OCT signal indicates that the injected LGNRs-PSS-mPEG remain stable *in vivo*. This is because the particles must retain their strong near-infrared scattering (i.e., remain stable and dispersed) in order to produce signal based on the OCT

detection bandwidth. A lack of LGNR aggregation is further evidenced by the health of the mouse during and after the experiment (the formation of μm-scale aggregates would have induced capillary blockage and subsequent embolism). However, the strongest evidence for LGNR-PSS-mPEG stability *in vivo* is provided by *ex vivo* analysis of mouse tissues collected 24 h post-injection. Hyperspectral microscopy of stained tissue sections revealed the intravascular presence of disperse puncta with spectra matching that of LGNRs (Figure S12, puncta are red). These red puncta are very likely LGNRs, as they are not observed within the tissues of uninjected mice. Both the size and spectra of these puncta indicated that the LGNRs retain their spectral properties and do not form large aggregates in the mouse blood vessels.

SUPPORTING DISCUSSION

Gold nanorods are known to exhibit shifts in plasmonic resonance following certain surface modifications.[S7] Such shifts can clearly be observed between LGNRs-CTAB and LGNRs-PSS as well as between GNRs-CTAB and GNRs-mPEG (Figure S5). Interestingly, LGNRs-CTAB and LGNRs-mPEG do not exhibit a plasmonic shift. This observation and the similarity of the particles' zeta potential trends during washing (Figure S4) make it somewhat difficult to confirm the successful coating of LGNRs-CTAB with mPEG-SH. However, DLS measurements demonstrate a clear increase in hydrodynamic diameter for LGNRs-mPEG relative to LGNRs-CTAB (Table S2), which suggests that the mPEG-SH coating step is indeed successful. The magnitude of this increase in diameter upon PEGylation is notably smaller than that observed from GNRs-CTAB to GNRs-mPEG, which indicates that the PEG coating on GNRs may be sufficiently denser than on LGNRs. The difference in coating density may be one factor that contributes to the stability of GNRs-mPEG and the instability of LGNRs-mPEG. Subsequent studies of PEG coating density may be performed in the future through high-resolution TEM imaging of heavy metal-stained samples.

The next step to understanding size-dependent stability requires an exploration of why GNRs and LGNRs may have different PEG coating densities. One answer lies in the nature of seed-mediated GNR synthesis itself. Original work by El-Sayed and Murphy suggested that the CTAB bilayer formed on GNRs during synthesis preferentially adsorbs along the longitudinal {100} faces of the particles while the growing end caps {111} remain relatively exposed.[S1,S2] It is this preferential adsorption that in fact enables anisotropic deposition of gold at the exposed ends that ultimately leads to the characteristic rod shape. After growth is complete, the residual CTAB remains bound along the longitudinal surface area while the end caps remain more accessible in solution. Thus, it is more likely from a kinetic standpoint for ligands such as PEG-SH to bind quickly to GNR ends rather than compete with CTAB on the longitudinal faces in a comparatively slow exchange reaction. Murphy *et al.* showed support for this hypothesis by demonstrating preferential end-to-end linkage of GNRs through biotin-streptavidin surface modifications.[S3] We independently demonstrated further evidence for this preference through TEM, Vis-NIR, and DLS studies of the binding of LGNRs-PEG-Biotin and GNRs-PEG-Biotin to NeutrAvidin-GNS (Figures S6-7, Table S3). GNS-NA are consistently found near the ends of LGNRs-PEG-Biotin in TEM images (Figure S6). One effect of this end-specific binding is a pseudo-increase in the GNR aspect ratio through surface plasmon hybridization effects.[S5,S6] Consistent with this theory, Vis-NIR measurements demonstrate significant red-shifting of LGNRs-PEG-Biotin incubated with GNS-NA relative to PEGylated LGNRs (Figure S7). While

one might expect to see little to no binding of GNS-NA to LGNRs-mPEG, TEM images indicate significant co-localization of these particles as well as clumping of multiple GNRs. The pattern of GNS-NA binding to LGNRs-mPEG is notably different from the pattern observed for LGNRs-PEG-Biotin. Specifically, there does not appear to be preferential association with LGNR-mPEG end caps. This observation, paired with the fact that multiple LGNRs-mPEG tend to clump together, is actually indicative of partial aggregation of bare gold surfaces rather than a PEG-specific binding interaction. Further evidence of this aggregation is observed as spectral broadening relative to free LGNRs-mPEG (Figure S7) and greatly increased particle hydrodynamic radius measured by DLS (Table S3). Unlike LGNRs-PEG-Biotin, GNRs-PEG-Biotin do not exhibit face-specific co-localization with GNS-NA, although general co-localization is observed relative to the incubation of GNS-NA with GNRs-mPEG (Figure S6). Plasmonic red-shifting is also observed for GNRs-PEG-Biotin when incubated with GNS-NA, while no such shifting is observed for GNRs-mPEG incubated with GNS-NA (Figure S7). DLS measurements also indicate successful GNRs-PEG-Biotin binding to GNS-NA through an increase in hydrodynamic diameter. Interestingly, GNRs-mPEG incubated with GNS-NA actually display lower average diameter than GNRs-mPEG alone, however this may be because the presence of free 10 nm spheres lowers the average particle diameter in bulk solution. Critically, the spectral broadening observed for LGNRs-mPEG with GNS-NA is not observed for GNRs-mPEG with GNS-NA (Figure S7). This observation provided further evidence that mPEG can successfully protect GNRs but not LGNRs from aggregation.

In light of these observations, it becomes more clear why GNRs and LGNRs coated with the same PEG-SH ligand may experience different colloidal stability. Calculations of atomic radius and bond length indicate that the maximum outstretched length of PEG_{5000}-SH is ~50 nm (given the worm-like chain behavior of linear polymers in solution, the actual average length is shorter than this upper limit). PEG_{5000} chains conjugated to the ends of GNRs (~50 x 15 nm) are, in theory, long enough to provide coating across the longitudinal faces of the GNR when excess CTAB is washed away. PEG_{5000} polymers at their persistence length in solution (~25 nm) may still provide coating to the majority of the GNR longitudinal surface area, as PEG is conjugated to both ends of the GNR (for more information regarding PEG_{5000} maximum length and persistence length, please see Reference S4). However, PEG_{5000} chains bound at the ends of LGNRs (~90 x 30 nm) are less capable of fully coating the longitudinal surfaces of the GNR. Thus, when excess CTAB is washed away, portions of bare gold are exposed along the particle surface. Inter-particle contact at these regions eventually leads to observed instability and aggregation.

In contrast with mPEG-SH, PSS is highly effective at stabilizing LGNRs as evidenced by Vis-NIR and zeta potential measurements (Figure 2-4, S2-4). There are several factors that may be responsible for conferring this stability. Primarily, PSS binds the LGNRs-CTAB surface through fundamentally different mechanisms. While mPEG-SH binds largely to the ends of GNRs through one covalent bond per molecule, PSS adheres to the LGNRs-CTAB surface through many ionic interactions (up to ~400 in theory for the 70 kDa polymer). Although these ionic interactions are weaker than the covalent Au-S bond that links PEG-SH with GNRs, the sheer number of ionic interactions between LGNRs-CTAB and PSS leads to excellent binding avidity effects and prolonged GNR stability. Because PSS can directly overcoat residual CTAB on the GNR surface, its binding is not limited to the ends of GNRs. Rather, PSS can provide a more complete particle overcoating. Once bound, PSS also provides effective GNR stability because

of active electrostatic repulsion among PSS polymers, whereas PEG-SH primarily conveys particle stability through weaker steric prevention of GNR surface fusion.

SUPPORTING FIGURES

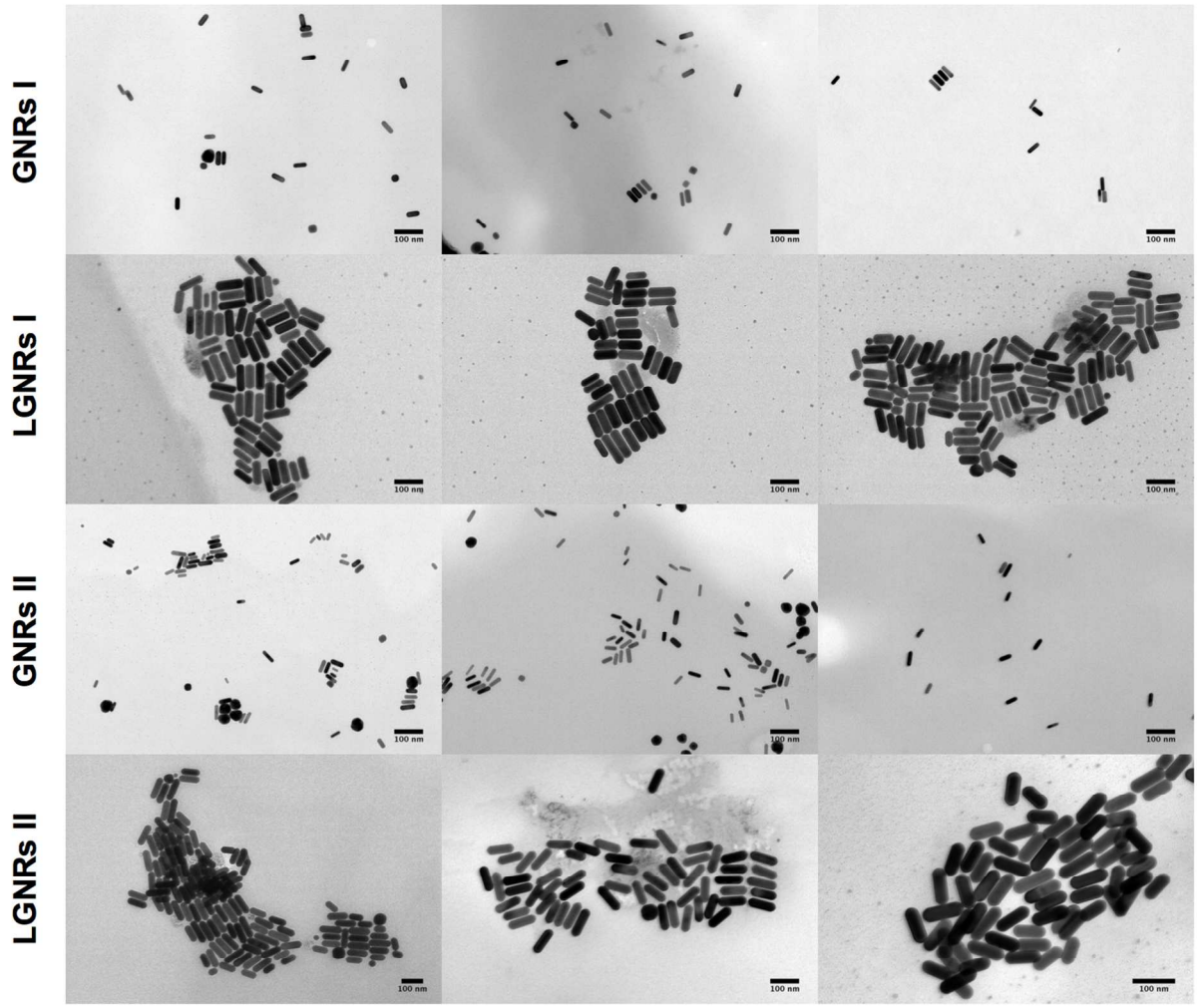

Figure S1. Additional TEM images used to calculate average GNR dimensions and aspect ratios. All scale bars are 100 nm.

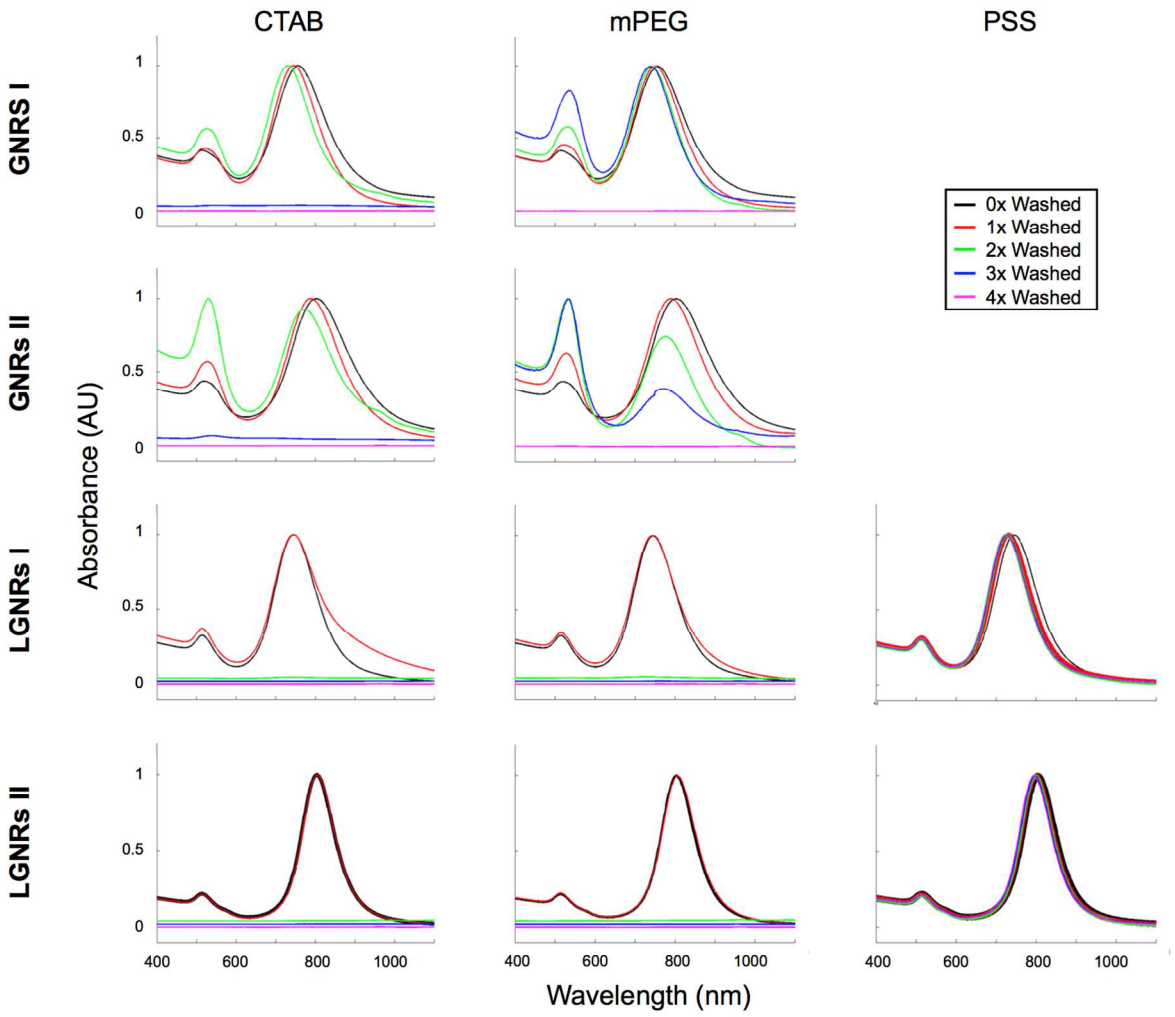

Figure S2. Original raw absorbance spectra measured for all GNRs, coatings, and wash cycles. Stability plots of $FWHM_0$ / $FWHM_n$ were derived from this data. Each plot contains the spectra from 0x wash (black), 1x wash (red), 2x wash (green), 3x wash (blue), and 4x wash (magenta) steps for the given particle size and coating. Absorbance spectra are peak normalized to account for material loss through pipetting and to clearly show when a given particle completely crashes out of solution (denoted by flat line). The increase in the transverse absorbance (~520 nm) for GNRs I and GNRS II is likely due to an enrichment of gold nanospheres during centrifugation (the spheres are larger and heavier than the GNRs, as evidence by TEM, so they pellet more efficiently). This effect is not observed for LGNRs due to a virtual lack of spherical particles and their increased weight (more efficient pelleting). Because (L)GNR stability was assayed through the FWHM of the longitudinal peak, this change in sphere concentration does not influence the stability measurements.

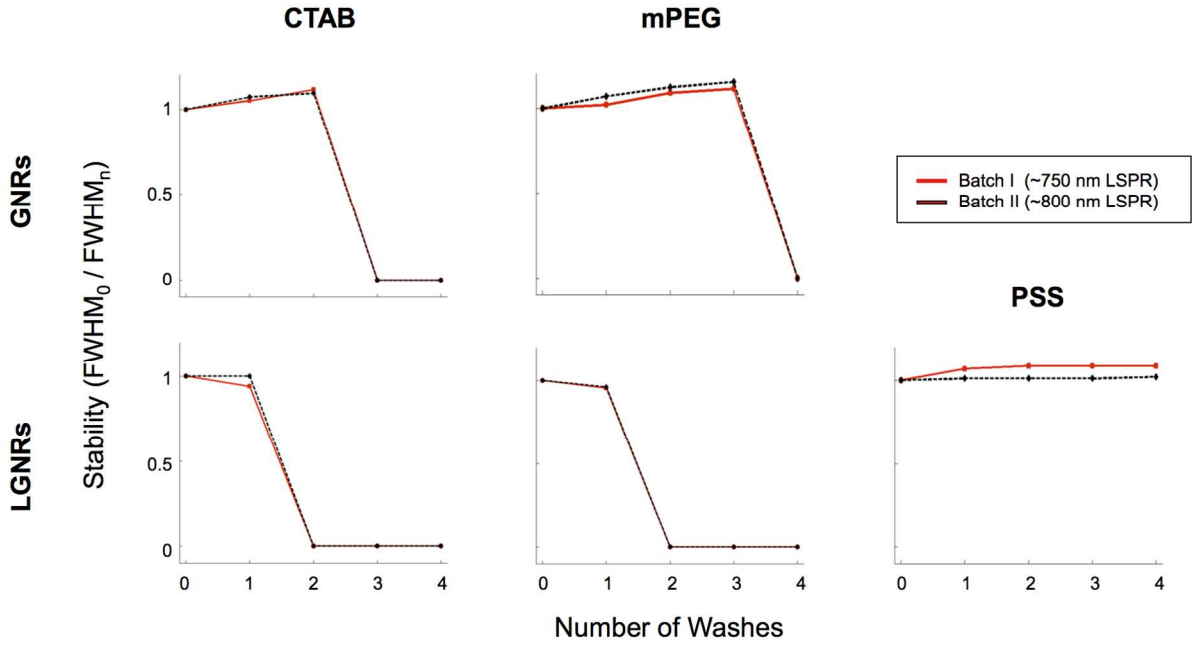

Figure S3. $FWHM_0$ / $FWHM_n$ stability plots for all GNRs used in this study. Note that stability trends for a given particle size and coating are consistent for Batch I and Batch II and thus independent of plasmonic properties.

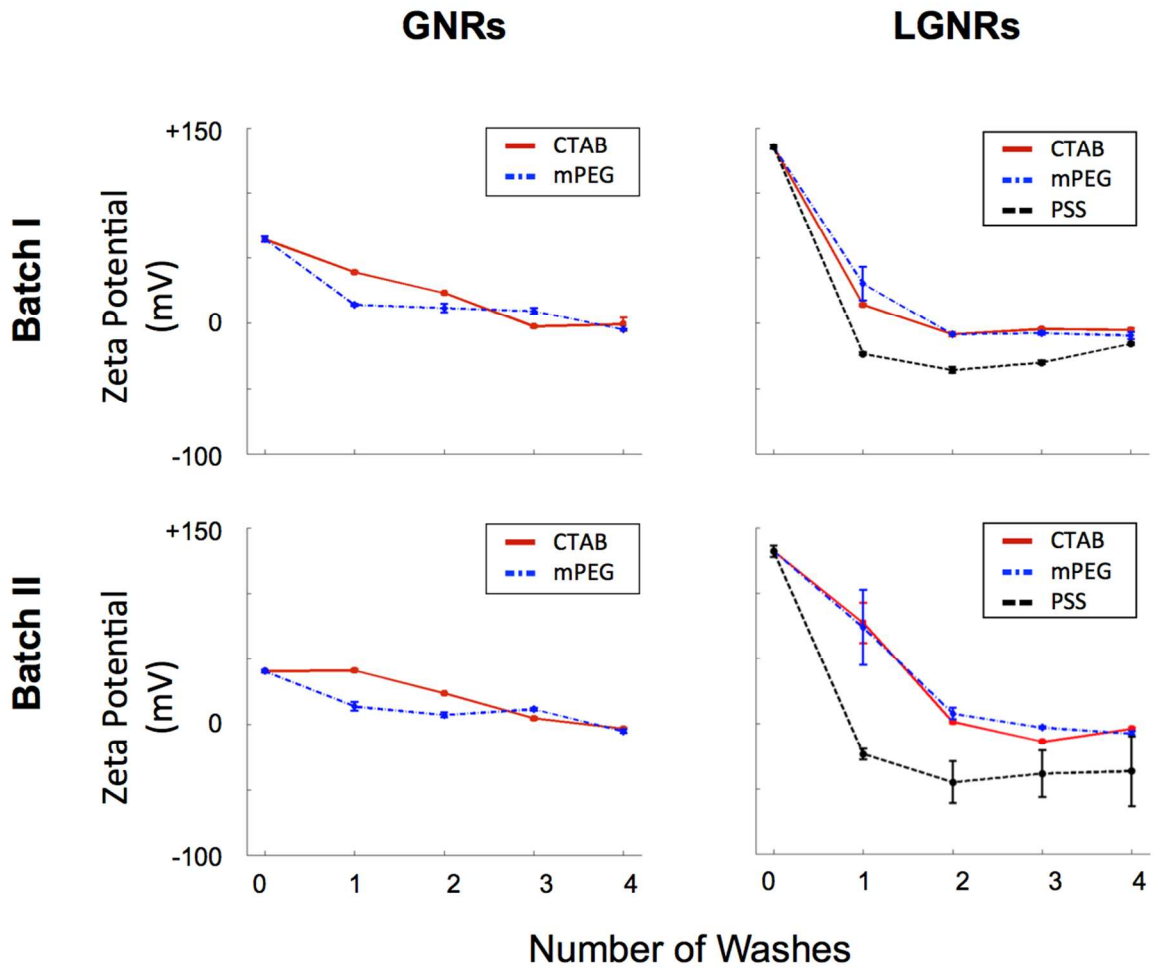

Figure S4. Zeta potential as a function of number of washes, particle size, and coating. All zeta potential measurements were performed in triplicate. Error bars represent standard error of the mean (s.e.m.) for each set of three measurements.

GNR	Wash #	CTAB	mPEG	PSS
GNRs I	0	+64 +/- 1.9 mV	---	---
	1	+39 +/- 0.7 mV	+14 +/- 0.8 mV	---
	2	+23 +/- 0.6 mV	+11 +/- 3.3 mV	---
	3	-2.8 +/- 0.6 mV	+9.1 +/- 2.2 mV	---
	4	-1.0 +/- 5.2 mV	-5.2 +/- 0.5 mV	---
GNRs II	0	+40 +/- 1.0 mV	---	---
	1	+41 +/- 0.8 mV	+13 +/- 3.3 mV	---
	2	+23 +/- 0.3 mV	+6.9 +/- 1.9 mV	---
	3	+4.4 +/- 0.7 mV	+11 +/- 1.0 mV	---
	4	-3.4 +/- 0.5 mV	-5.4 +/- 1.4 mV	---
LGNRs I	0	+135 +/- 1.7 mV	---	---
	1	+14 +/- 0.9 mV	+30 +/- 13 mV	-24 +/- 1.0 mV
	2	-8.8 +/- 1.7 mV	-8.7 +/- 0.4 mV	-36 +/- 2.3 mV
	3	-4.9 +/- 0.6 mV	-8.0 +/- 1.1 mV	-30 +/- 1.5 mV
	4	-5.4 +/- 1.0 mV	-10 +/- 2.9 mV	-16 +/- 1.2 mV
LGNRs II	0	+132 +/- 4.3 mV	---	---
	1	+77 +/- 16 mV	+73 +/- 29 mV	-24 +/- 4.1 mV
	2	+1.2 +/- 0.9 mV	+7.3 +/- 4.3 mV	-45 +/- 16 mV
	3	-14 +/- 0.4 mV	-3.2 +/- 0.7 mV	-39 +/- 18 mV
	4	-4.0 +/- 0.8 mV	-8.0 +/- 1.9 mV	-37 +/- 27 mV

Table S1. Original zeta potential measurements. Values are presented as mean zeta potential from triplicate measurements ± standard error of the mean (s.e.m.).

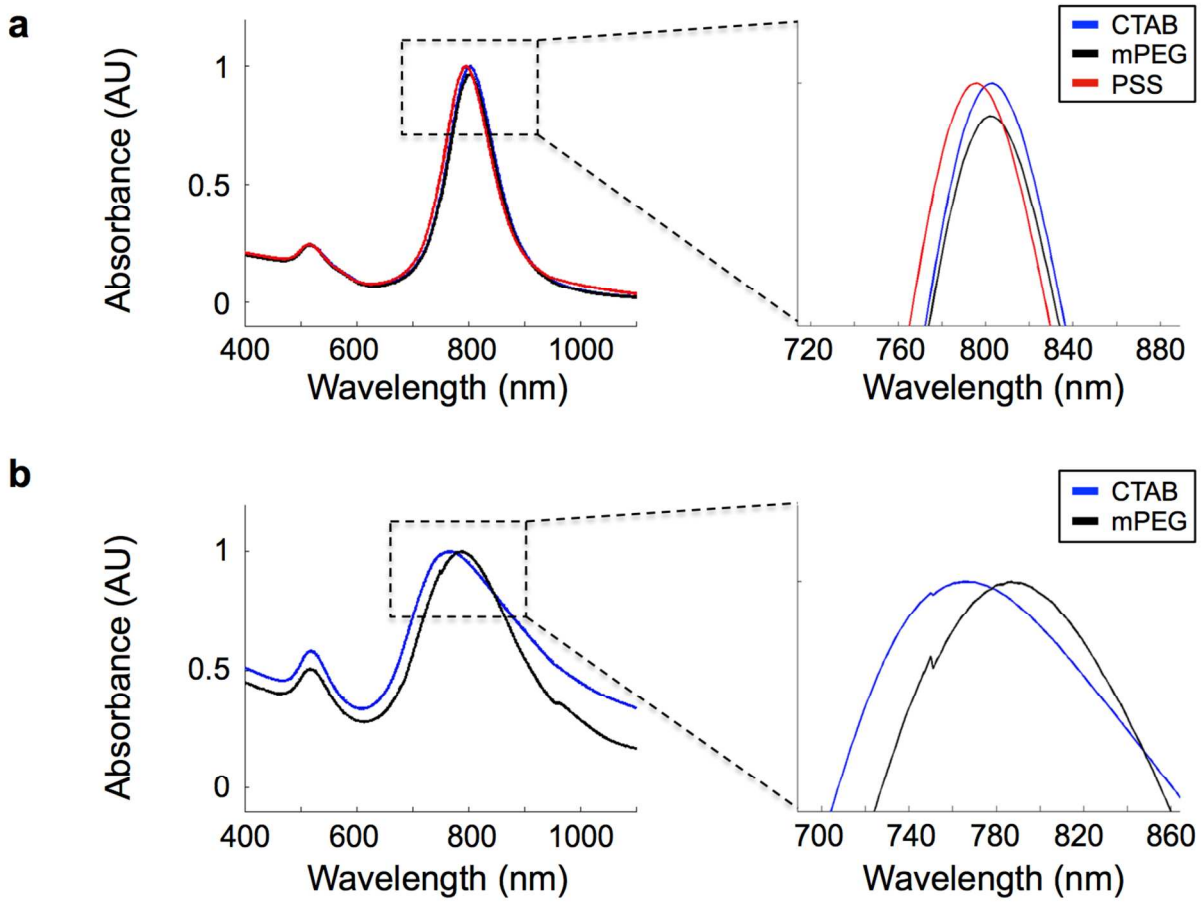

Figure S5. Changes in Vis-NIR absorbance spectra of GNRs with different surface coatings. **(a)** LGNRs-CTAB and LGNRs-mPEG exhibit nearly identical plasmonic peaks while LGNRs-PSS exhibit ~10 nm blue-shifting. **(b)** GNRs-mPEG exhibit ~20 nm red-shifting compared to the original stock of GNRs-CTAB.

Hydrodynamic Diameter (nm)

	CTAB	mPEG	PSS
LGNRs	25.8 ± 0.4	34.6 ± 0.5	60.1 ± 0.8
GNRs	20.4 ± 0.2	61.6 ± 7.1	---

Table S2. DLS measurements of GNR hydrodynamic radii confirm successful surface coating. LGNRs-CTAB exhibit an increase in hydrodynamic diameter following incubation with mPEG-SH, consistent with successful surface modification. LGNRs-CTAB incubated with PSS show an ever greater increase in diameter, suggesting that PSS provides a thicker or more complete coating that mPEG for LGNRs. GNRs also exhibit a significant increase in diameter upon incubation of mPEG-SH. Interestingly, this increase is much greater relative to that observed for LGNRs-mPEG. All measurements were performed in triplicate, and all values are presented as mean +/- standard deviation derived from scattering intensity.

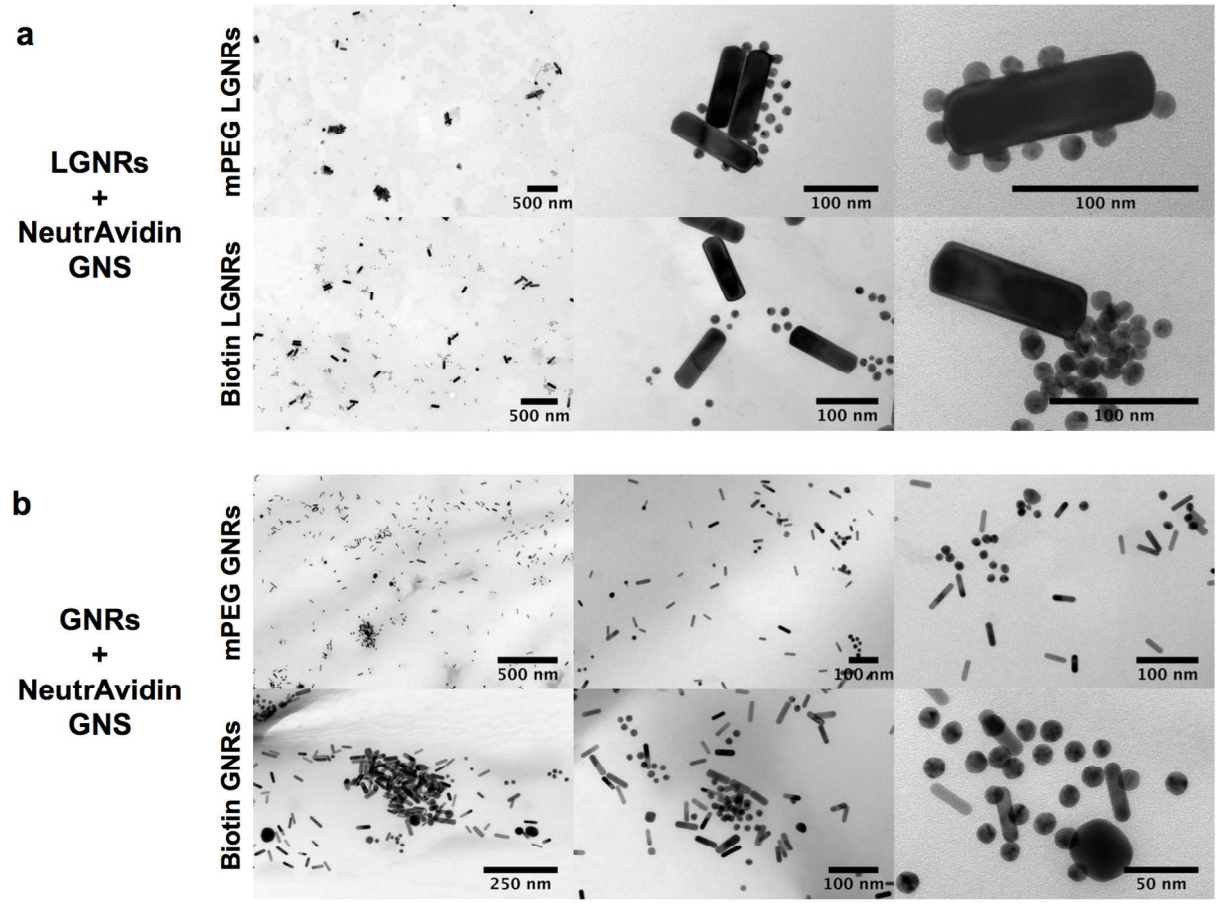

Figure S6. TEM images show that GNRs coated with mPEG-SH or Biotin-PEG-SH interact with NeutrAvidin-coated GNS in distinct ways. **(a)** NA-GNS bind in uniform fashion to all faces of LGNRs-mPEG suggesting non-specific association. Early signs of particle aggregation are also evident in this sample as clumps of LGNRs and GNS (top row). In contrast, NA-GNS appear more frequently near the end facets of LGNRs-PEG-Biotin. The ends of (L)GNRs are expected to bind more PEG-SH than longitudinal facets, consistent with TEM observations (bottom row). **(b)** GNRs-mPEG do not obviously co-localize with NA-GNS through either aggregation or specific binding (top row), while GNRs-PEG-Biotin do exhibit co-localization with NA-GNS. Unlike LGNRs-PEG-Biotin incubated with NA-GNS, the co-localization of NA-GNS with GNRs-PEG-Biotin is not facet-specific (bottom row).

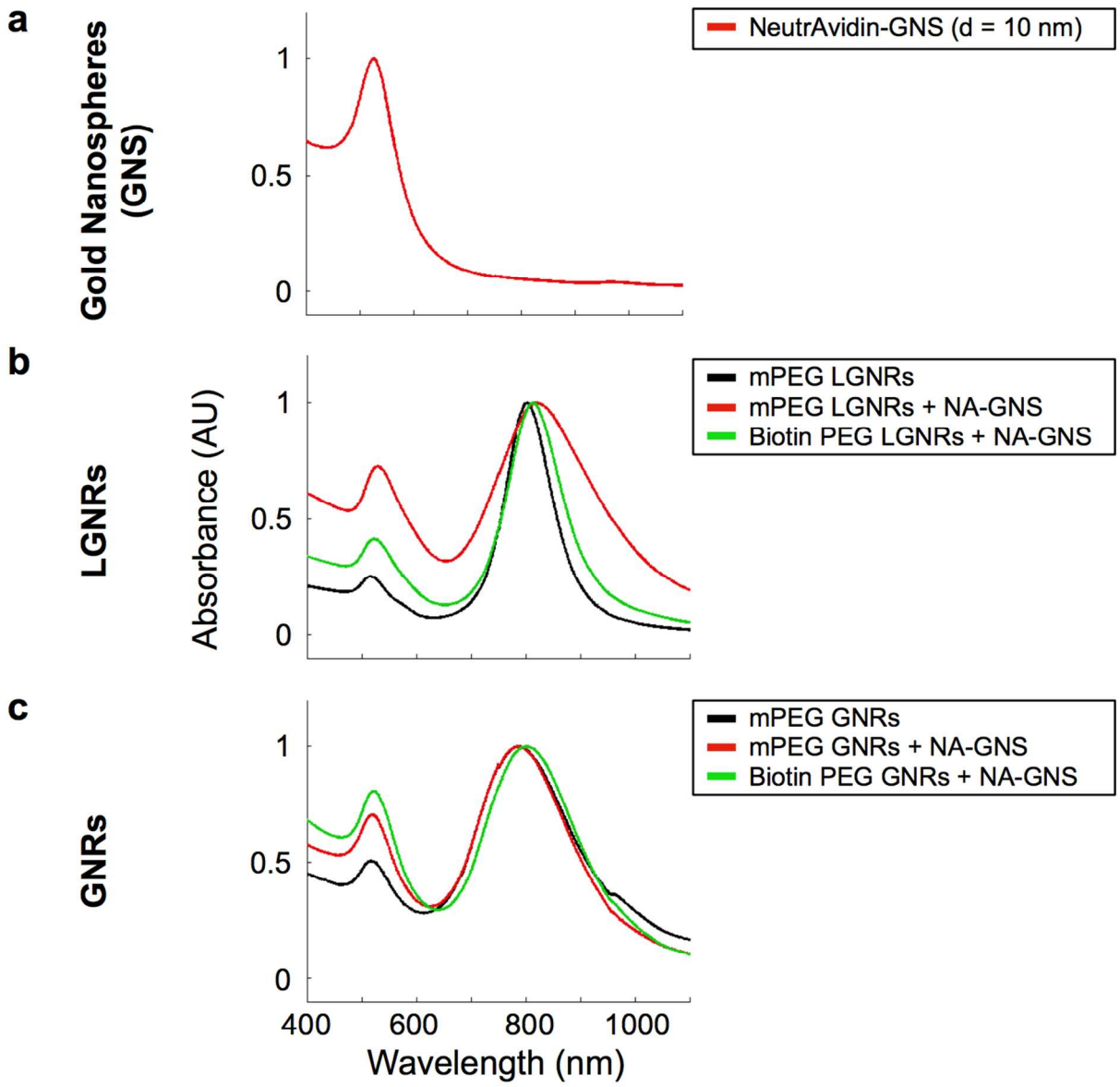

Figure S7. Spectral measurements of GNR-GNS incubations are consistent with observations from TEM with respect to PEG binding and GNR stability. **(a)** 10 nm NA-GNS incubation with LGNRs-mPEG exhibited red shifting and spectral broadening relative to free LGNRs mPEG. **(b)** By contrast, LGNRs-PEG-Biotin incubated with NA-GNS exhibited red-shifting but no broadening, indicative of plasmon hybridization due to preferential GNS binding to the LGNR end caps. **(c)** GNRs-mPEG exhibit no peak broadening or red-shifting upon incubation with NA-GNS, but GNRs-PEG-Biotin red-shift ~20 nm after NA-GNS incubation, consistent with the behavior observed for LGNRs-PEG-Biotin.

Hydrodynamic Diameter (nm)

	mPEG GNRs Only	mPEG GNRs + NA-GNS	Biotin PEG GNRs + NA-GNS
LGNRs	34.6 ± 0.5	408 ± 5.4	127 ± 0.6

Table S3. DLS measurements of GNR-GNS incubations further corroborate TEM and Vis-NIR results. LGNRs-mPEG incubated with NA-GNS show a major increase in hydrodynamic diameter, consistent with the formation of the small aggregates observed directly in TEM and inferred from spectral peak broadening. LGNRs-PEG-Biotin also exhibited a greater diameter that free PEGylated LGNRs, consistent with GNS binding.

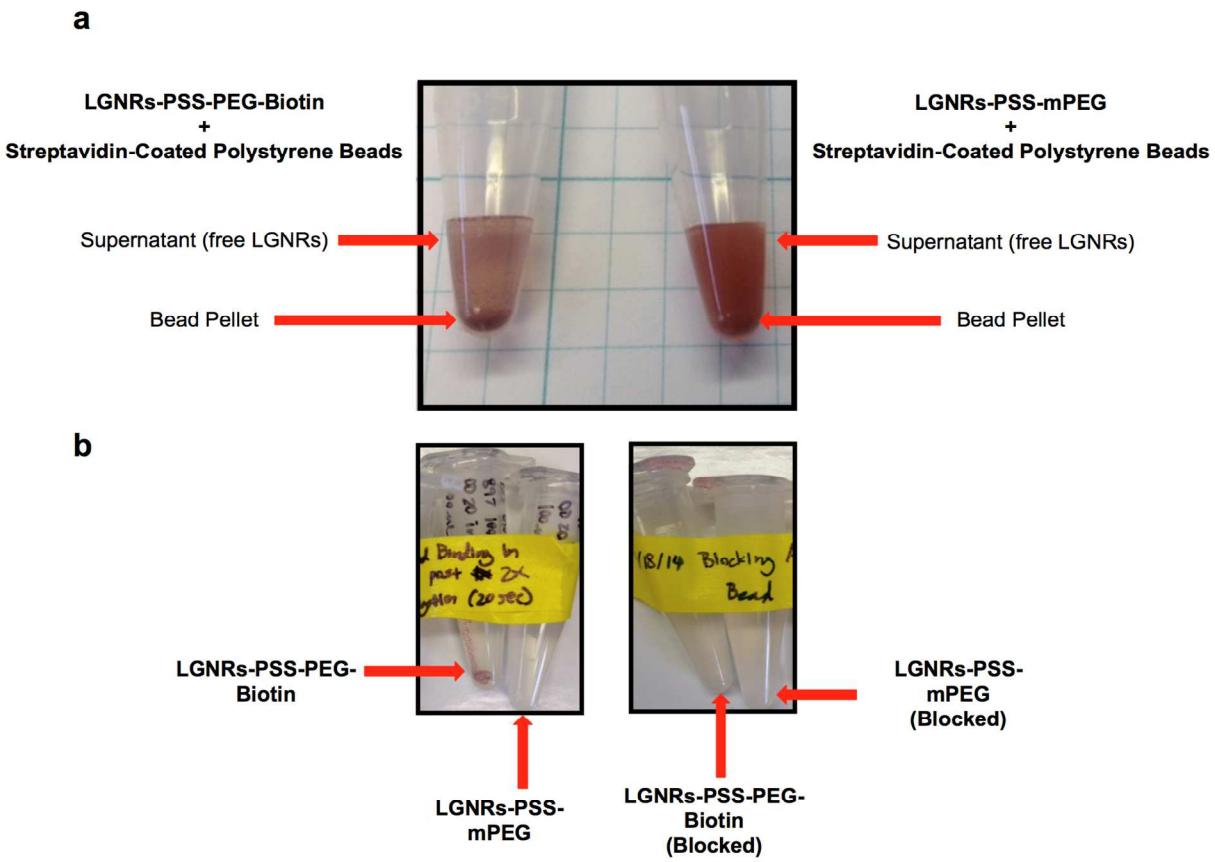

Figure S8. Qualitative visual assessment of GNR-bead binding and blocking assays. **(a)** LGNRs-PSS-PEG-Biotin bind streptavidin-coated beads, resulting in a red bead pellet and reduced GNR concentration in the supernatant. LGNRs-PSS-mPEG are incapable of specific binding to streptavidin coated beads, and the majority of these GNRs remain free in solution rather than bound to beads in the pellet. **(b)** Washing bead pellets post-incubation further demonstrates the binding specificity of LGNRs-PSS-PEG-Biotin. The red pellet is clearly visible for the LGNRs-PSS-PEG-Biotin + streptavidin bead incubation while the pellet remains white when GNRs lack a biotin coating (left). No red pellet occurs for either GNR type if the streptavidin beads are pre-blocked with free biotin (right).

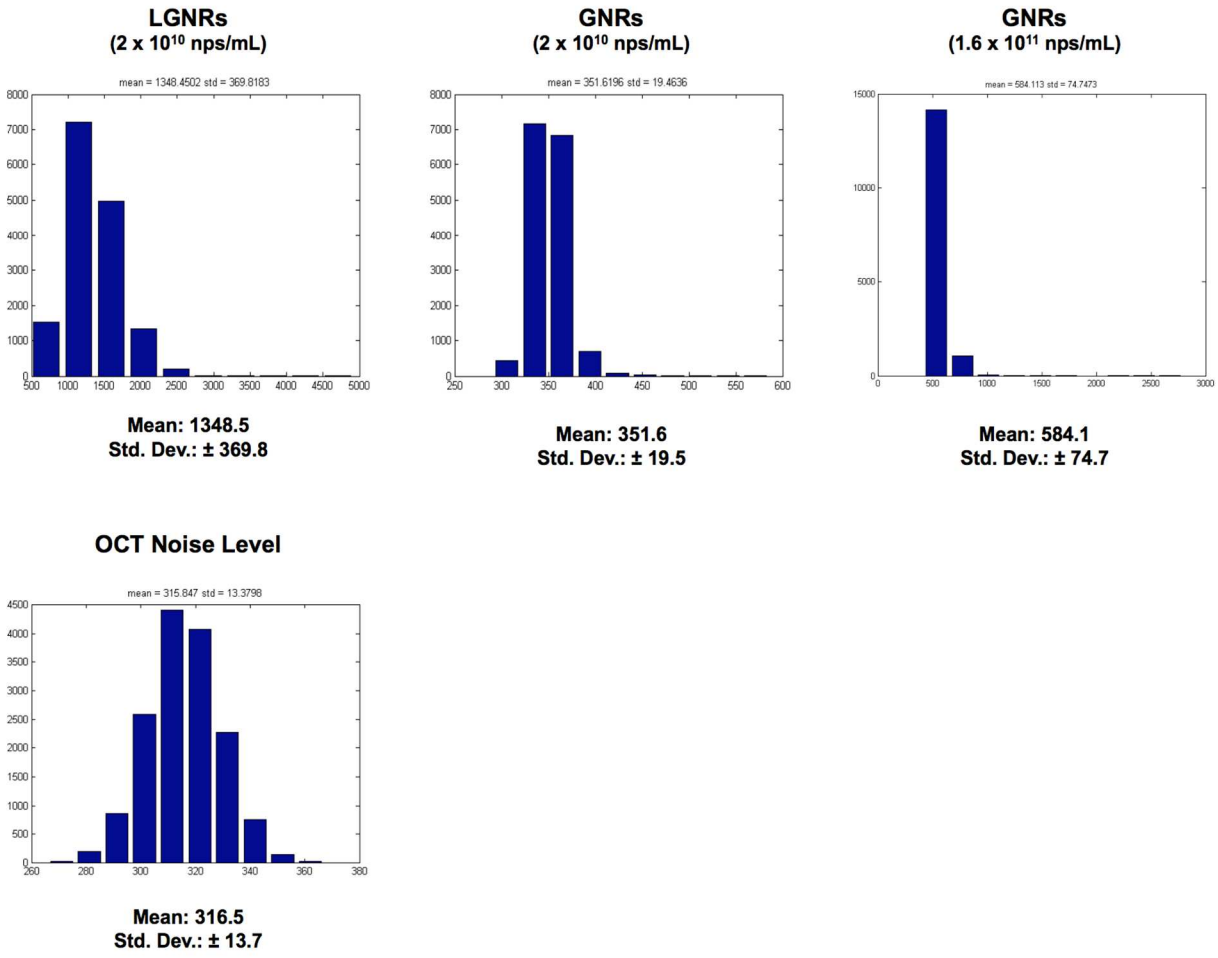

Figure S9. Pixel intensity distributions and mean OCT signal ± standard deviation of LGNRs and GNRs from analyzed regions of interest (ROIs, n = 15,000 pixels each). This data was used to calculate statistical significance and relative OCT signal strength for LGNRs and GNRs at equivalent concentrations (OD and nps/mL). The OCT system's noise level was also quantified. All ROIs were taken at the same focal depth and relative location within (L)GNR sample tubes to minimize aberrant differences in signal intensity.

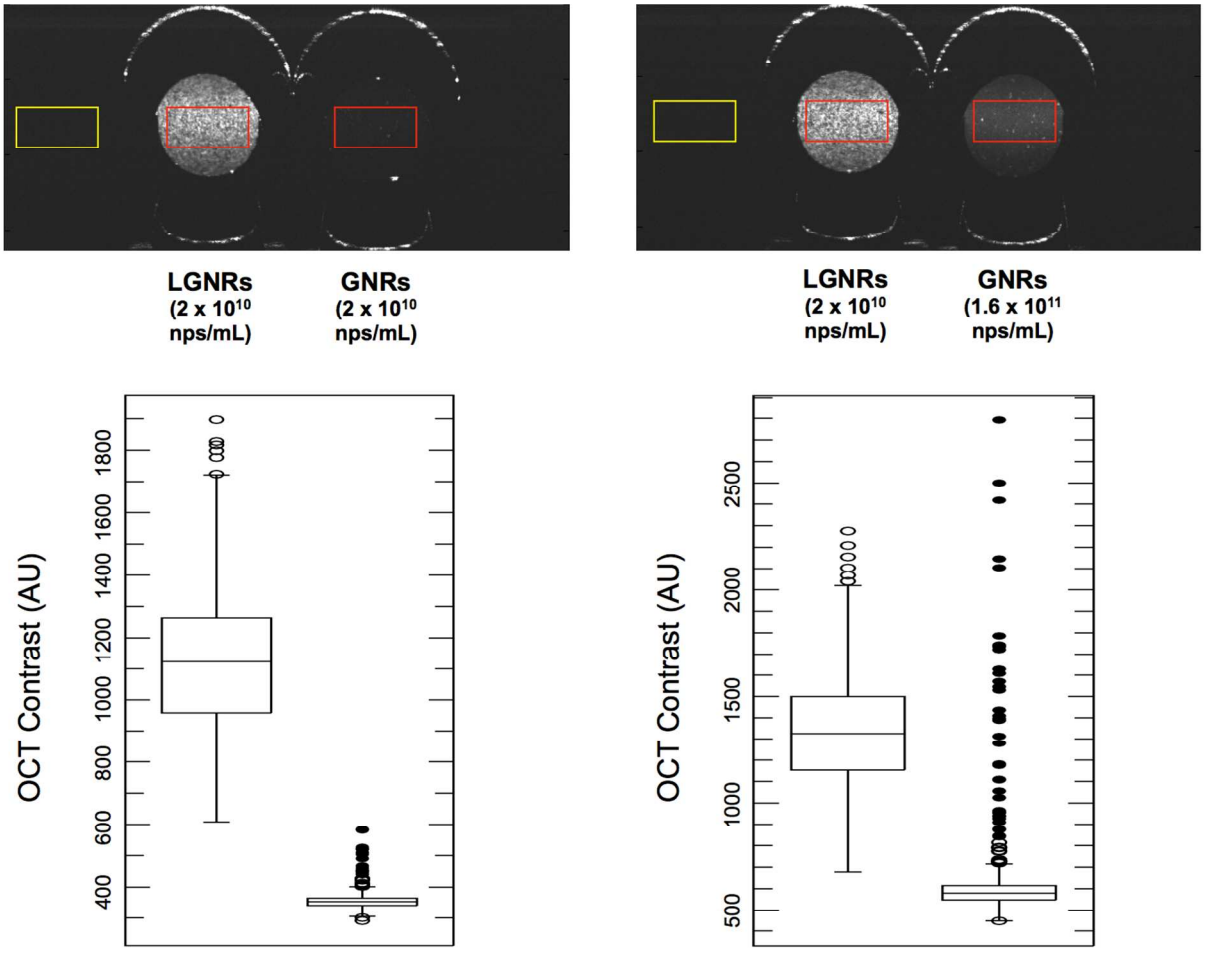

Figure S10. Original OCT images of LGNRs vs GNRs at equivalent nps/mL (left) and equivalent OD (right). 600 pixel subsets of the original 15,000 pixel ROIs (shown as red rectangles for GNR samples and yellow rectangles for noise regions)were taken from each sample to determine the statistical significance of the difference in signal between LGNRs and GNRs. Two-tailed Student's t-tests were performed to compare LGNRs vs GNRs in each case. Box plots from each comparison are presented below their respective OCT images. In each case, OCT signal from LGNRs is markedly greater than from GNRs ($p < 0.0001$).

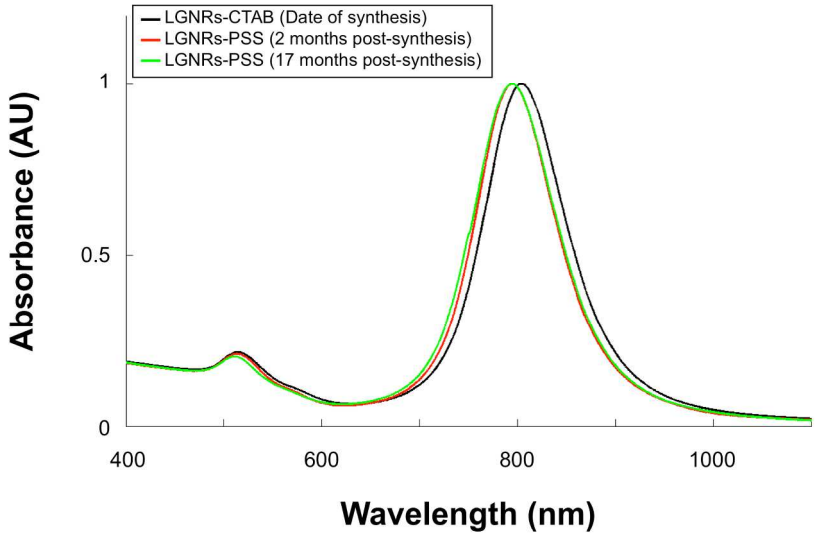

Figure S11. LGNRs exhibit long-term stability ("shelf-life"). Vis-NIR spectra of the same LGNR sample were measured immediately following synthesis (black curve), immediately following LGNR surface functionalization with PSS (red curve; for this sample, as-synthesized LGNRs-CTAB were stored for 2 months at room temperature prior to PSS coating), and after long-term storage at 4°C (green curve; acquired 15 months after surface functionalization, i.e., 17 months post-synthesis). After over a year of storage, LGNRs-PSS exhibited nearly identical spectral properties and purity as on the day they were first coated with PSS.

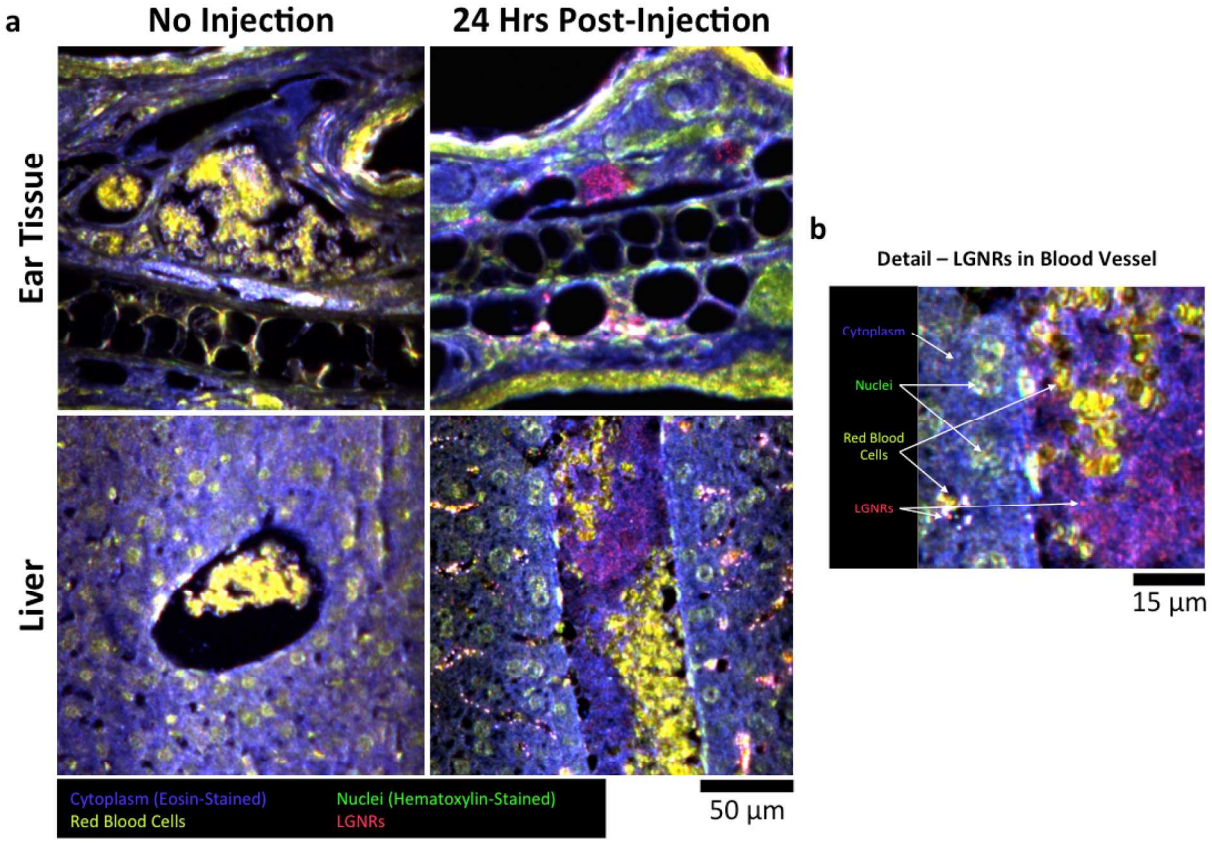

Figure S12. LGNRs-PSS-mPEG remain monodisperse and stable during *in vivo* use. (**a**) Tissue sections (ear and liver) were collected from control mice (no LGNRs-PSS injection) and from mice intravenously injected with LGNRs-PSS (sections were collected 24 h post-injection). These sections were stained with Hematoxylin and Eosin (H&E) and imaged using a hyperspectral dark-field microscope (CytoViva, Auburn, AL). False-coloring the images according to detected wavelength-dependent scattering enables clear observation of cell nuclei (green), red blood cells (yellow), cytoplasm (blue), and LGNRs (red). The bottom-right image in (a) shows a blood vessel running through the mouse liver, as denoted by the presence of both red blood cells and LGNRs-PSS. (**b**) Detailed observation of tissue sections reveals that individual LGNRs-PSS (red puncta) can be distinguished. We expect that these puncta are in fact single LGNRs-PSS based on their apparent size (in some cases no larger than a single pixel, which is ~400nm) as well as the fact these pixels exhibit unique near-infrared scattering peaks with narrow FWHM values.

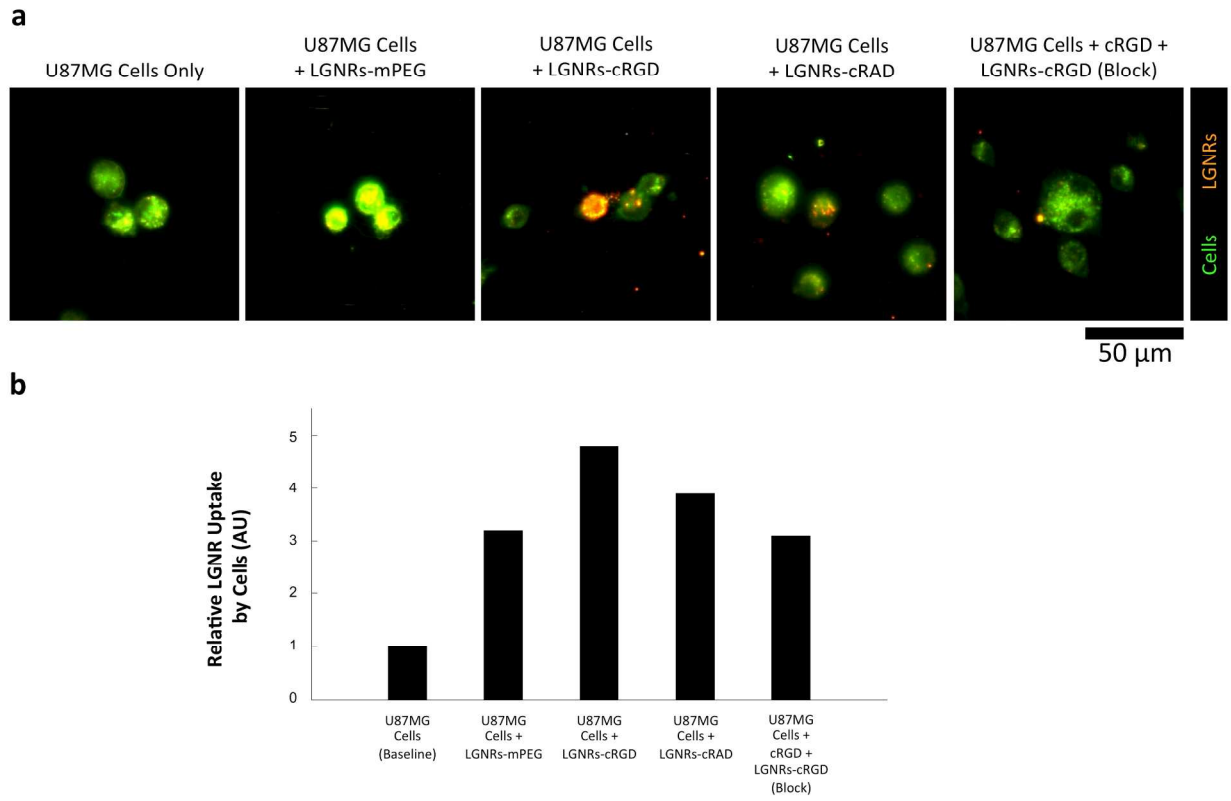

Figure S13. Demonstration of molecular specificity for LGNRs-PSS conjugated with targeting biomolecules. (**a**) U87MG cells were incubated with LGNRs-PSS conjugated with mPEG-SH, cRGD, or cRAD (a cRGD structural analog with low binding specificity to $\alpha_V\beta_3$ integrin). The greatest cellular uptake is observed for the targeted particles (LGNRs-cRGD). Non-specific particles (LGNRs-mPEG and LGNRs-cRAD) exhibit lower cellular uptake, potentially due to a lack of molecular binding specificity. As evidenced in the far-right panel, cells pre-incubated with free cRGD (blocking assay) have minimal uptake of LGNRs-cRGD. These results suggest that LGNR-cRGD binding to the U87MG cells is at least in part due to molecularly specific binding. (**b**) Comparison of the relative LGNR uptake for each cell incubation condition. Values represent the intensity-normalized average LGNR signal per cell (n=3 cells for each sample). While LGNRs-cRGD exhibit the most cellular uptake, it is interesting to note the heterogeneity of LGNR uptake. This may be due in part to cell-to-cell variation in $\alpha_V\beta_3$ expression and potentially cell-to-cell variations in viability.

SUPPORTING REFERENCES

(S1) Nikoobakht, B.; El-Sayed, M. A. *Langmuir* **2001**, *17*, 6368-6374.
(S2) Gao, J.; Bender, C. M.; Murphy, C. J. *Langmuir* **2003,** *19*, 9065-9070.
(S3) Caswell, K. K.; Wilson, J. N.; Bunz, U. H. F.; Murphy, C. J. *J. Am. Chem. Soc.* **2003**, *125*, 13914-13915.
(S4) Choi, C. H. J.,; Zuckerman, J. E.; Webster, P.; Davis, M. E. *Proc. Natl. Acad. Sci.* **2011**, *108*, 6656-6661.
(S5) Pramod, P.; Joseph, S. T. S.; Thomas, K. G. *J. Am. Chem. Soc.* **2007**, *129*, 6712-6713.
(S6) Funston, A. M.; Novo, C.; Davis, T. J.; Mulvaney, P. *Nano Lett.* **2009**, *9*, 1651-1658.
(S7) Rostro-Kohanloo, B. C.; Bickford, L. R.; Payne, C. M.; Day, E. S.; Anderson, L. J. E.; Zhong, M.; Lee, S.; Mayer, K. M.; Zal, T.; Adam, L.; Dinney, C. P. N.; Drezek, R. A.; West, J. L.; Hafner, J. H. *Nanotechnology* **2009**, *20*, 434005.